IEEE Access
Multidisciplinary ⁝ Rapid Review ⁝ Open Access Journal

Received July 10, 2018, accepted August 17, 2018, date of publication August 29, 2018, date of current version September 21, 2018.

Digital Object Identifier 10.1109/ACCESS.2018.2867456

Band Pass Filters Based on GaN/Si Lumped-Element SAW Resonators Operating at Frequencies Above 5 GHz

DAN NECULOIU[1,2], (Member, IEEE), ALINA-CRISTINA BUNEA[1], (Member, IEEE), ADRIAN M. DINESCU[1], AND LEO A. FARHAT[3]

[1]National Institute for Research and Development in Microtechnologies, 077190 Bucharest, Romania
[2]Faculty of Electronics, Telecommunications and Information Technology, Politehnica University of Bucharest, 060042 Bucharest, Romania
[3]European Space Agency, 2200 AG Noordwijk, The Netherlands

Corresponding author: Alina-Cristina Bunea (alina.bunea@imt.ro)

This work was supported in part by the Romanian Ministry of Research and Innovation under Project PN-III-P2-2.1-PED-2016-0976 and in part by the European Space Agency under Contract 40000115202/ 15/NL/CBi.

ABSTRACT This paper reports on a GaN/Si surface acoustic wave (SAW) impedance element filter operating in the few gigahertz region. The PI-type filter consists of three SAW resonators with the same digit/interdigit widths, integrated with series/parallel planar inductors. The design procedure is based on modeling the SAW resonators using four parameters, independent of the equivalent circuit model representation (series resonance frequency, static capacitance, quality factor, and effective coupling coefficient). The series frequency is tuned by a planar inductor placed in series, while the parallel resonant frequency is tuned by a planar inductor placed in parallel with the SAW resonator. Closed-form equations are derived for the analysis of lumped-element SAW resonators. The design procedure is further based on the area of the SAW resonator and the lengths of the planar inductors as independent variables. Full-wave electromagnetic and circuital co-simulations and parametric optimizations are employed for the final filter design, which is implemented in the coplanar waveguide topology. The lumped-element SAW bandpass filter is fabricated using e-beam lithography for the definition of the 200-nm-wide interdigital transducers. Measurement results show the insertion losses of 12.9 dB at 5.49 GHz, the return losses of 16 dB, 3-dB bandwidth of 8.3 MHz, and the out-of-band rejection of 24 dB. The filter is compatible with monolithic integration with GaN active electronics.

INDEX TERMS Band-pass filters, coplanar waveguide, effective coupling coefficient, gallium nitride, piezoelectric transducers, SAW filters.

I. INTRODUCTION

In the last decade Gallium nitride (GaN) has become the most popular material after silicon (Si) in the semiconductor industry [1]. It is a wide bandgap semiconductor with good piezoelectric properties and can be grown with high quality on silicon substrates. Using a (AlGaN/GaN) stack on silicon it is possible to make a heterostructure with a 2D electron gas and high electron mobility transistors (HEMT). These GaN HEMTs have excellent low noise or high power performances in the microwave frequency range.

To exploit GaN at its full potential in advanced microwave monolithic integrated circuits (MMICs) it is very important to integrate passive devices (such as resonators and filters), sensors (temperature, gas, pressure, etc.) and other functional devices with GaN active electronics.

Due to the progress in the epitaxial growth of GaN on silicon technologies, it has become feasible to implement devices such as surface acoustic wave (SAW) devices operating at frequencies higher than 5 GHz [2]. Published work for these high operating frequencies is focused on temperature [3] and pressure sensors [4].

For filter applications, most research efforts have been concentrated on other piezoelectric materials such as aluminium nitride (AlN) [5], zinc oxide (ZnO), lead zirconate titanate (PZT) or quartz [6], [7]. But these materials, although they exhibit excellent piezoelectric properties are

2169-3536 © 2018 IEEE. Translations and content mining are permitted for academic research only.
Personal use is also permitted, but republication/redistribution requires IEEE permission.
See http://www.ieee.org/publications_standards/publications/rights/index.html for more information.

not semiconductor materials such as GaN. It is this property that enables the monolithic integration and full compatibility of GaN with active devices such as HEMTs.

Only few results can be found in the literature related to microwave SAW filters on GaN. In [8] delay lines processed on iron doped GaN grown on sapphire show dual transmission at 237.8 MHz and 349.7 MHz, with insertion losses of around 24-25 dB. A silicon membrane (thickness 10 μm) supported resonator with an operating frequency of 2.1 GHz and insertion losses of 14 dB was reported in [9]. Palacios *et al.* reported a GaN on sapphire device in [10] operating at 1.625 GHz and 2.25 GHz, with insertion losses of 23 dB and 15 dB, respectively. Another delay line type device was reported in [2], with an operating frequency of 5.64 GHz and insertion losses of 33 dB.

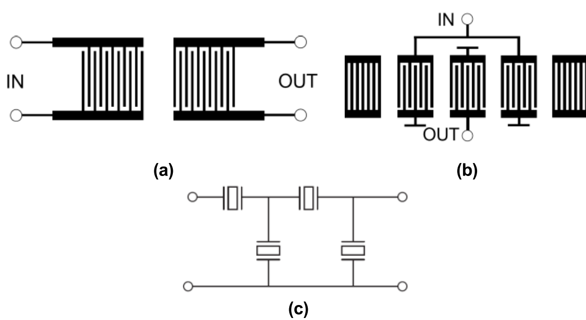

FIGURE 1. Common SAW based band-pass filter configurations: (a) delay line; (b) longitudinally-coupled resonator filters; (c) impedance element filters.

Common SAW based band-pass filters (BPF) include: delay line type filters (Fig. 1(a)); longitudinally-coupled resonator (LCR) filters (Fig. 1(b)) and impedance element filters (ladder filters) (Fig. 1(c)). As presented above, the delay line type filters on GaN have high insertion losses and the losses increase with frequency [1]. The LCR filters require either vias connection to ground (in microstrip topology) or wire connection (in coplanar waveguide topology). This adds parasitic elements which cannot be controlled by design but will greatly influence the filter response.

The approach used in this paper is based on the impedance element filters (IEF) (Fig. 1(c)). This approach requires a strict control of the series and parallel resonance frequencies of the SAW resonators. The effective coupling coefficient of GaN/Si resonators strongly depends on the propagation modes, and for SAWs is limited to a maximum value of 0.9% [1], which leads to a difference between the two resonance frequencies of few MHz. The basic operating principle of an IEF requires that the series resonance frequency of one SAW resonator is equal to the parallel resonance frequency of the nearby SAW resonator. Neither the variation of the metallization thickness nor the variation of the digit/interdigit width can provide such an accurate control [11].

In [12] a new family of RF band pass filters based on hybrid acoustic wave lumped element resonators is proposed. Unlike traditional acoustic wave filter topologies, the SAW resonators in the filter have the same resonance frequency. The concept was used in [13] for the design of a BPF with the coupling-matrix based approach and in [14] for the realization of constant in-band group-delay BPF and diplexers. The reported filters were designed for quasi-elliptic frequency response using appropriate techniques. They are based on discrete commercial SAW resonators hybrid integrated with lumped inductors and capacitors (surface mount devices) on the same printed circuit board (PCB). Typically, a lumped inductor is connected in parallel with the SAW resonator in order to introduce two symmetric transmission zeros in the frequency response. The operating frequency was well below 1 GHz, limited by the parasitic elements specific to the integration approach.

For the case of GaN/Si SAW resonators, series connected planar inductors with values between 0.2-1 nH were used to tune the series resonance frequency of SAW resonators in the 5.4 – 8.6 GHz range [15].

This paper reports a new approach for obtaining GaN/Si SAW band pass filters operating in the few GHz region. It is based on planar inductors for the independent control of the series and parallel resonance frequencies. For the lumped-element SAW resonator, an inductor placed in series can tune the series resonance frequency without affecting the parallel resonance frequency; an inductor placed in parallel can control the parallel resonance frequency, while the series resonance will be unaffected. All the SAW resonators in the proposed filter have the same series/parallel resonance frequencies. Using a new modeling approach for the SAW resonator structure, based on 4 model parameters originating from its physical behavior, the area of each resonator becomes an important independent variable in the design, together with the planar inductors layout. Because of the relative high operating frequency, full-wave electromagnetic simulations are required for accurate design and optimization of the filter layout implemented in the coplanar waveguide topology.

The paper is organized as follows. Section II presents the SAW resonators modeling using four parameters originating from the physical behavior of the resonator structure that are independent of the equivalent circuit model representation. They are the series resonance frequency (f_s), the static capacitance (C_o), the effective coupling coefficient (k^2_{eff}) and the mechanical quality factor (Q_m). The analysis of the effect of series and parallel connected inductors on the series and parallel resonance frequencies is investigated by new proposed closed form equations. Section III describes the technological process used to fabricate SAW resonator test structures and the proposed filter. The four main model parameters are extracted from measured data as a function of the SAW resonator area. Section IV introduces the design procedure based on full-wave electromagnetic and circuital co-simulations and parametric optimizations. The layout of a PI-type band pass filter with lumped element SAW resonators, operating at a frequency of about 5.5 GHz is presented.

Finally, the designed filter is fabricated, measured and the filter performances are presented. After a slight change of the

model parameters used in the design, the agreement between the simulated and experimental data is excellent.

II. LUMPED-ELEMENT SAW BASED RESONATORS MODELING

A. SAW RESONATOR MODELING

Since the acoustic waves speed is more than four orders of magnitude lower than the electromagnetic waves speed, piezoelectric structures (like SAW resonators) can be modeled in the electric domain using (1). In the mechanical domain the structure is modeled by Newton's equation of motion (2). The electric and mechanical domains are coupled by the piezoelectric effect represented by the constitutive equations (3).

$$divD = 0 \tag{1}$$

where D is the dielectric displacement.

$$\nabla T = \rho \frac{\partial^2 u}{\partial t^2} \tag{2}$$

where T is the mechanical stress, ∇ is the divergence operator, u is the mechanical displacement, t is the time and ρ is the mass density.

$$\begin{aligned} T &= c_E S - e^T E \\ D &= eS + \varepsilon_S E \end{aligned} \tag{3}$$

where S is the mechanical strain, E is the electric field, c_E are the stiffness parameters at constant electric field, ε_S are the dielectric coefficients at constant strain, e are the piezoelectric coefficients.

The solution of the equation system (1)-(3) depends on the geometry of the structure, boundary conditions (in both mechanical and electrical domains) and on the material parameters.

A surface acoustic wave can be generated and received using an interdigital transducer (IDT). The applied voltage between the alternately connected electrodes produces a spatially periodic electric field and a periodic strain field. A draft of the cross section of the IDT is presented in Fig. 2, where w is the digit (electrode) width and s is the separation of two digits.

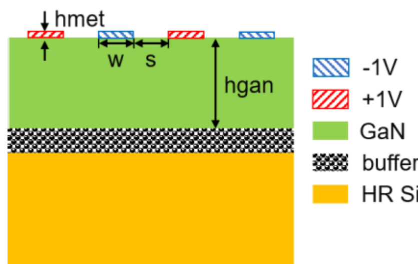

FIGURE 2. Cross section of two pairs of IDTs and substrate layer configuration.

Two pairs of electrodes are represented. The electrodes are placed on a GaN layer with the thickness *hgan*, grown on a buffer layer on a high resistivity (HR) silicon substrate. The alternated applied voltage gives rise to a SAW that propagates in both directions with wave fronts parallel to the IDT digits.

The maximum wave amplitude is obtained when constructive interference among the digits occurs. This happens for frequencies where the acoustic wavelength is equal to the transducer period $2 * (w + s)$. For a single resonator, the resonance frequency f_{res} is given by (4), where v_{ph} is the phase velocity of the acoustic wave.

$$v_{\text{ph}} = 2\,(w + s)\,f_{\text{res}} \tag{4}$$

The surface acoustic wave propagation and generation is well documented in the literature (see [6], [7], [16]–[18]).

The phase velocity (v_{ph}) depends on the layer structure, the material properties and the propagation mode. For the GaN on silicon configuration used in this work the equations were solved using a FEM based commercial software package (COMSOL Multiphysics) and the results were presented in [11]. Different propagation modes with different phase velocities were identified. At the resonance frequency f_{res} (defined in (4)) the electrical signal frequency matches the electro-mechanical resonance frequency of the structure. Due to the piezoelectric effect, the charged particle displacement is very large causing an increase in the electrical current flowing through the IDT electrodes resulting in a minimum of the impedance.

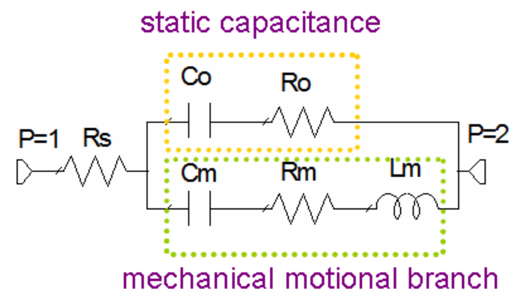

FIGURE 3. Modified Butterworth Van-Dyke SAW resonator equivalent circuit.

For filter design, a more compact, time efficient modeling technique is required. One practical solution is the modified Butterworth Van-Dyke (mBVD) lumped elements equivalent circuit (Fig. 3) [19]. The circuit consists of a mechanical motional branch with the motional resistance (R_m), motional capacitance (C_m) and motional inductance (L_m) connected in series and the static capacitance (C_o) connected in parallel. Two loss resistors R_s and R_o were added to the equivalent circuit to model the conductive losses in the digit electrodes and the losses in the dielectric layers, respectively.

If the losses are neglected, the equivalent impedance (Z) of the circuit is given by (5). The series resonance frequency $\omega_s = 2\pi f_s$ (corresponding to the maximum of the magnitude of the admittance) and the parallel resonance frequency $\omega_p = 2\pi f_p$ (corresponding to the maximum of the magnitude

of the impedance) are given by (6) and (7), respectively.

$$Z = \frac{j\omega L_m \left(1 - \frac{\omega_s^2}{\omega^2}\right)}{\left(1 + L_m C_0 \omega_s^2\right)\left(\frac{\omega^2}{\omega_p^2} - 1\right)} \quad (5)$$

$$\omega_s^2 = \frac{1}{C_m L_m} \quad (6)$$

$$\omega_p^2 = \left(1 + \frac{C_m}{C_0}\right)\omega_s^2 \quad (7)$$

The losses present in real materials determine a certain degree of uncertainty in the definition of these frequencies. In [20] f_s corresponds to the maximum device conductance and f_p is defined as the frequency of the maximum resistance. For a low loss and low effective coupling coefficient resonator the other two associated frequencies (from [20]), the resonance frequencies f_m(corresponding to maximum admittance) and f_n (corresponding to maximum impedance) are practically equal to f_s and f_p, respectively. These definitions are independent of the lumped elements equivalent circuit and can be used for every piezoelectric resonator. As a consequence, $f_s \cong f_{res}$.

The equivalent circuit from Fig.3 has 6 independent variables as model parameters and is used to design SAW resonator based circuits, including band-pass filters hybrid integrated with lumped components. The main disadvantage of this approach is its low generic applicability, since the 6 parameters are not directly linked to a given layer structure (like GaN on Si, for example) and device geometry (area, digits width and separation).

In this paper, a new modeling approach of SAW resonators based on 4 main independent parameters is proposed. This is used for the design of monolithically integrated SAW resonator based filters. These parameters originate from the physical behavior of the resonator structure and are independent of the equivalent circuit model representation. They are the series resonance frequency (f_s), the static capacitance (C_o), the effective coupling coefficient (k_{eff}^2) and the mechanical quality factor (Q_m). Other two secondary parameters, R_s and R_o (conductive losses in the IDT digits and dielectric losses in the GaN layer, respectively) will be added to the model in the later stages of the design.

The series resonance frequency was described above. It depends on the acoustic wave phase velocity (for the corresponding propagation mode) and on the geometric parameters w and s. This frequency does not depend on the area of the SAW resonator which is proportional to the digit length.

For frequencies much lower than f_s or much higher than f_p, the IDT structure is characterized by its static capacitance C_o. This parameter models the electric field distribution in the structure, and hence the electric energy storage. The static capacitance will linearly depend on the digit length, therefore on the area of the SAW resonator. Due to the edge effect there will be a static capacitance component independent of digit length that will be proportional to the number of digits.

The effective coupling coefficient k_{eff}^2 is a measure of the ratio between electric field energy density and the mechanical energy density in the IDT. It is related to the strain distribution and to the electric field distribution in the device [21]. As a consequence, the parameter depends on the propagation mode of the SAW. This parameter is affected not only by the material properties, but also by the layer structure and thickness, electrodes width and thickness, piezoelectric and metallic thin films quality, etc. It is expected that this parameter should have a slight dependence on the area of the SAW resonator. At the digits edges there are electric field components that are not parallel with the SAW propagation direction and contribute only to the electric field energy.

A convenient measure of the effective coupling coefficient used in filter design is given by (8) [20]. Because of the small value of the k_{eff}^2 for the GaN/Si SAW resonators, it can be related to the mBVD equivalent circuit parameters by (9), for $C_m \ll C_o$.

$$k_{eff}^2 = \frac{f_p^2 - f_s^2}{f_p^2} \quad (8)$$

$$k_{eff}^2 = \frac{\frac{C_m}{C_0}}{1 + \frac{C_m}{C_0}} \cong \frac{C_m}{C_0} \quad (9)$$

The mechanical quality factor Q_m is a measure of the energy dissipation in the resonator due to acoustic losses (viscous losses, acoustic wave scattering, acoustic wave leakage in the substrate, etc) and piezoelectric conversion losses. Using the mBVD equivalent circuit model, Q_m is defined at $\omega_s = 2\pi \cdot f_s$ by (10). Note that the motional inductance Lm is a measure of the mechanical energy stored in the resonator. This parameter is affected by the piezoelectric material quality and by the quality of the IDT's metallization. It is independent of the device area.

$$Q_m = \frac{\omega_s L_m}{R_m} \quad (10)$$

The numerical modeling of the SAW resonator structure using FEM gives only a first estimation of the model parameter values, not accurate enough to be used in the filter design. Therefore, experimental work is needed. Test structures with SAW resonators placed in series on a CPW transmission line (TL) with different areas have been fabricated, measured and the model parameters were extracted. The results are presented in Section III.B.

B. SERIES AND PARALLEL LUMPED-ELEMENT SAW RESONATORS

The IEF topology is a cascade of SAW resonators in series connection (horizontally placed along the transmission path) and SAW resonators parallel-connected (vertically placed along the transmission path). The topology selected in this work is the PI-type filter shown in Fig.4 (a) [7]. The general theory for the IEF design requires the fulfillment of the

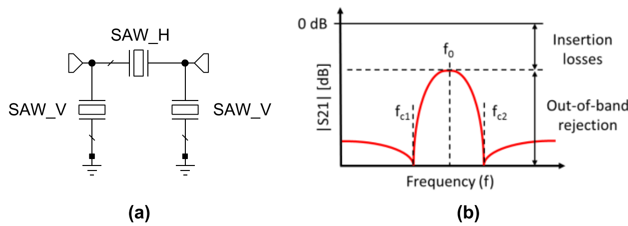

FIGURE 4. (a) Pi-type filter configuration; (b) frequency response and the definition of filter main parameters.

conditions given by (11) for the SAW resonators (Fig. 4 (b))

$$\begin{cases} f_{s,SAW_H} = f_0 \\ f_{p,SAW_H} = f_{c2} > f_0 \\ f_{p,SAW_V} = f_0 \\ f_{s,SAW_V} = f_{c1} < f_0 \end{cases} \tag{11}$$

where: f_s and f_p are the series and parallel resonance frequencies of the corresponding SAW resonators, f_o is the filter central operating frequency, f_{c1} is the lower maximum rejection frequency and f_{c2} is the upper maximum rejection frequency.

This approach requires a strict control of the series and parallel resonance frequencies of the SAW resonators. The effective coupling coefficient of the SAW processed on GaN/Si is limited to a value of at most 0.1%, which leads to a difference between the two resonance frequencies of a few MHz. Numerical simulations confirmed by experimental results showed that it is very difficult to accurately control the series and the parallel resonance frequencies by means of the IDT width, aspect ratio or metallization thickness. The simulated control rate is 5 MHz/nm for the electrode thickness and 0.7 MHz/nm for the electrode width [11], far away from the technology capabilities.

The new approach reported in this paper consists of using inductors for the independent control of the series and parallel resonance frequencies. An inductor placed in series with the SAW resonator can tune the series resonance frequency without affecting the parallel resonance frequency [15]. An inductor placed in parallel with a SAW resonator, connected in series on the signal path can control the parallel resonance frequency (which corresponds to transmission zeros [12]) while the series resonance will be unaffected.

The equivalent circuit of an inductor L_{ser} placed in series with the SAW resonator is shown in Fig.5 (a). Neglecting the losses, the SAW resonator is described by (5). The parallel resonance frequency (maximum of impedance magnitude) is not affected. After some algebraic manipulation, the two equivalent series resonance frequencies (minimum of impedance magnitude) are given by (12). A new characteristic frequency ω_o is introduced as a function of L_{ser} (13). The result is valid for $L_m \gg L_{ser}$, which is the case for the SAW resonators processed on GaN/Si presented in this work. The two solutions from (12) are represented in normalized form in Fig.5(b) for an effective coupling

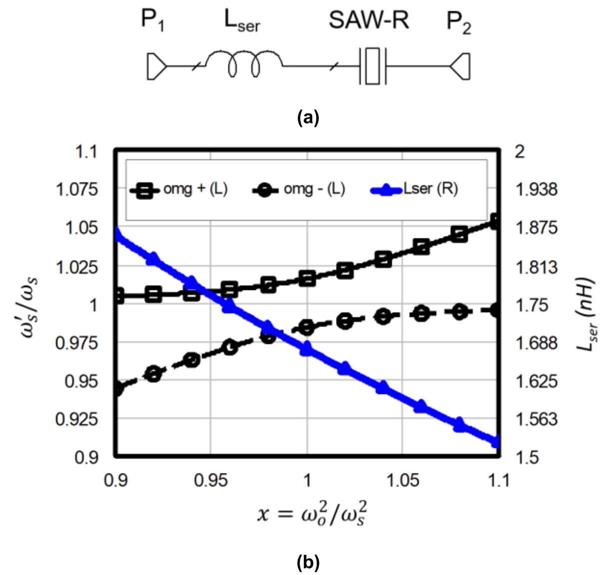

FIGURE 5. (a) Circuit schematic of the SAW resonator in series with the inductor Lser; (b) Normalized solutions for series resonance frequencies and the corresponding values of L_{ser} ($k_{eff}^2 = 0.1\%$, $C_o = 0.5$ pF).

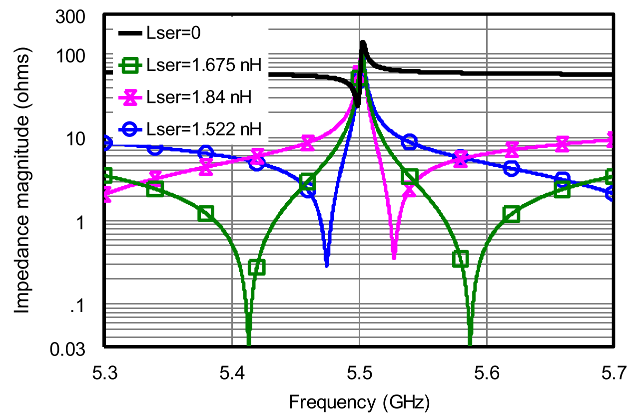

FIGURE 6. Magnitude of the equivalent impedance with L_{ser} as parameter ($f_s = 5.5$ GHz, $k_{eff}^2 = 0.1\%$, $C_o = 0.5$ pF, $Q_m = 2000$).

coefficient of $k_{eff}^2 = 0.1\%$. The x axis is $x = \omega_o^2/\omega_s^2$ and the vertical axis is $y = \omega'^2_s/\omega_s^2$. For $x = 1$ the relative change in the series resonance frequency is about $+/-$ 1.6 %. The necessary L_{ser} value for the relative series resonance frequency shift is also shown in Fig. 5(b) for a static capacitance of $C_o = 0.5$ pF.

$$\omega_s'^2 \cong \frac{1}{2}\left[\omega_0^2 + \omega_p^2 \pm \sqrt{\frac{\left(\omega_p^2 - \omega_0^2\right)^2 + \frac{C_m}{C_0}\left(\omega_0^2 + \omega_p^2\right)^2}{1 + \frac{C_m}{C_0}}}\right] \tag{12}$$

$$\omega_0^2 = \frac{1}{L_{ser}C_0} \tag{13}$$

The circuit from Fig.5 (a) was analyzed using NI AWR Microwave Office (AWR MWO – www.awrcorp.com) and

the magnitude of the impedance is represented in Fig.6 for $L_{ser} = 0$ nH and other 3 representative values from Fig.5(b). The SAW resonator has the parameters: $f_s = 5.5$ GHz, $C_o = 0.5$ pF, $k^2_{eff} = 0.1\%$, $Q_m = 2000$ (corresponding to $L_m = 1675$ nH, $C_m = 0.5$ fF and $R_m = 29\ \Omega$) and R_s and R_o are zero. The parallel resonance frequency (maximum of impedance magnitude) is almost constant and the series resonance (minimum of impedance magnitude) is controlled by the L_{ser} value.

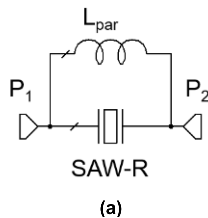

(a)

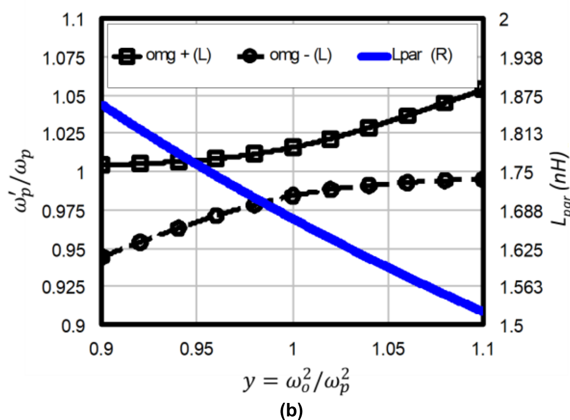

(b)

FIGURE 7. (a) Circuit schematic of the SAW resonator in parallel with the inductor Lpar; (b) Normalized solutions for parallel resonance frequencies and the corresponding values of L_{par} ($k^2_{eff} = 0.1\%$, $C_o = 0.5$ pF).

The equivalent circuit of an inductor L_{par} placed in parallel with the SAW resonator is shown in Fig.7 (a). The SAW resonator is described by (5) and two equivalent parallel resonance frequencies are calculated as (14) for $L_m \gg L_{par}$. A similar result was reported in [12], but the result (14) has a more compact closed form. The similarity between (12) and (14) is not surprising, since they are the solution of an equation of the type $Z(\omega)+j\omega L = 0$. The series resonance frequency is not affected by L_{par}. The characteristic frequency ω_o is a function of L_{par} (15). The two solutions from (14) are represented in normalized form in Fig.7 (b) for an effective coupling coefficient of $k^2_{eff} = 0.1\%$, for ω_o close to ω_p. The required value for L_{par} for a relative parallel resonance frequency shift is also shown in Fig.7 (b) for a static capacitance of $C_o = 0.5$ pF.

The circuit from Fig.7 (a) was analyzed using AWR MWO and the magnitude of its impedance is represented in Fig.8 for no parallel inductor and other 3 representative values for L_{par}. The SAW resonator has the same parameters as above ($f_s = 5.5$ GHz, $C_o = 0.5$ pF, $k^2_{eff} = 0.1\%$, $Q_m = 2000$) and the conductive/dielectric losses are neglected. The series

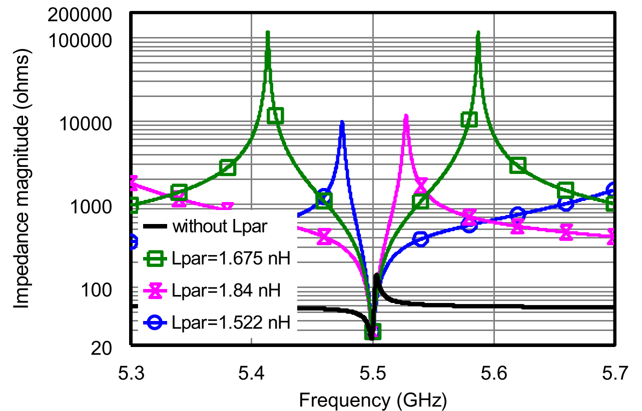

FIGURE 8. Magnitude of the equivalent impedance with L_{par} as parameter ($f_s = 5.5$ GHz, $k^2_{eff} = 0.1\%$, $C_o = 0.5$ pF, $Q_m = 2000$).

resonance frequency (minimum of impedance magnitude) is almost constant and the parallel resonance (maximum of impedance magnitude) is controlled by the L_{par} value.

$$\omega_p'^2 \cong \frac{1}{2}\left[\omega_0^2+\omega_p^2 \pm \sqrt{\frac{\left(\omega_p^2-\omega_0^2\right)^2+\frac{C_m}{C_0}\left(\omega_0^2+\omega_p^2\right)^2}{1+\frac{C_m}{C_0}}}\right] \tag{14}$$

$$\omega_0^2 = \frac{1}{L_{par}C_0} \tag{15}$$

III. FABRICATION OF SAW RESONATOR BASED CIRCUITS

A. TECHNOLOGICAL FLOW

Lumped-element SAW resonators were fabricated using a combination of electron beam lithography (EBL) and standard mask-based photolithography on a GaN/Silicon substrate acquired on custom request from the supplier NTT-AT Japan (http://www.ntt-at.com). The undoped GaN (Wurtzite crystal structure) layer has a thickness of 1 μm and is grown on a AlN buffer through MetalOrganic Chemical Vapor Deposition (MOCVD). The silicon wafer has a (111) crystallographic orientation and a resistivity $>$5kΩ·cm.

The patterning of the test structures was performed in a three step process. First, the large metal areas (CPW-TL and planar inductors) and alignment marks were patterned using lift-off of Ti/Au (5 nm/150 nm). This step was followed by the EBL of the 200 nm wide IDTs and deposition of Ti/Au (5 nm/95 nm). In the last step, an overlay metallization was deposited (Ti/Au – 5 nm/150 nm), covering the large metal areas and part of the IDT contact electrodes. This metal sandwich ensures a good contact between the thin IDT metallization and the thicker CPW-TLs. For the EBL the Raith e-Line equipment was used, combined with a PMMA 950k A4 resist. The metallization was done through e-beam evaporation in the Temescal FC 2000 installation. Due to the electrical isolation properties of

the undoped GaN layer, negative charging can occur during the e-beam process, which limits the writing field to an area of 100x100 μm^2.

B. SAW RESONATORS PARAMETER EXTRACTION

Test SAW resonators with various IDT areas were placed in series on coplanar waveguide (CPW) transmission lines for experimental characterization and the extraction of equivalent circuit parameters. The connecting CPW lines have the gap-signal-gap of 50-100-50 μm corresponding to a characteristic impedance close to 50 Ω.

The test structures were fabricated and the S parameters were measured on-wafer using a Vector Network Analyzer from Anritsu. A standard SOLT (short-open-load-thru) calibration was performed.

The SAW resonators were modeled with the mBVD equivalent circuit (Fig.3) using the model parameters introduced in Section II.A. These parameters were extracted from S-parameter measurements, using the optimization routines implemented in AWR MWO. The error function was defined as the difference between the measured S-parameters and those calculated for the equivalent circuit, for the current model parameters. The SAW resonator structure measured S parameters were carefully de-embedded using the "2-Port Negation Element" feature of AWR MWO.

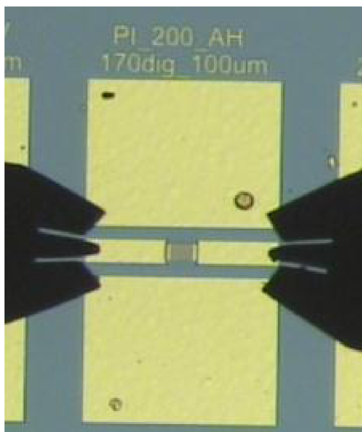

FIGURE 9. Photo of fabricated series connected SAW resonator with 170 digits of 100 micrometer length and 200 nm digit/interdigit width.

A photo of a fabricated test structure with 170 digits of 100 μm length is presented in Fig. 9. In this case, the digit width and separation were $w = s = 200$ nm for a target series frequency of 5.5 GHz. The measured and simulated S-parameters for the extracted parameter set is given in Fig. 10 and the excellent agreement validates the accuracy of the extracted parameters.

The model parameters extracted for different areas are shown in Fig.11 (a)-(c).

The area is calculated as the product of the digit length, the number of digits and the sum of the digit and interdigit widths. Ten test structures were measured for each area

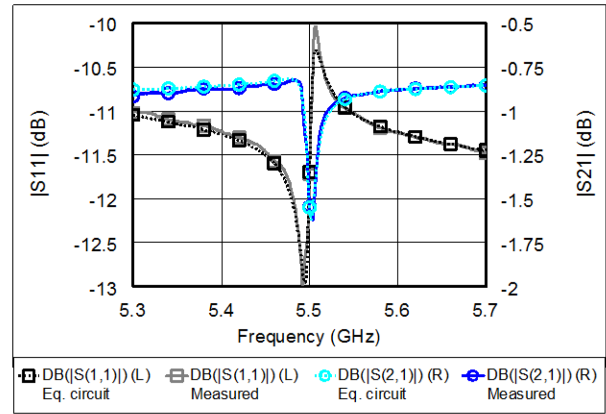

FIGURE 10. Measured and simulated S parameters for the test structure from Fig.9.

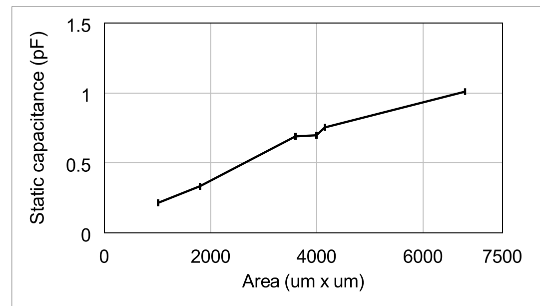

(a)

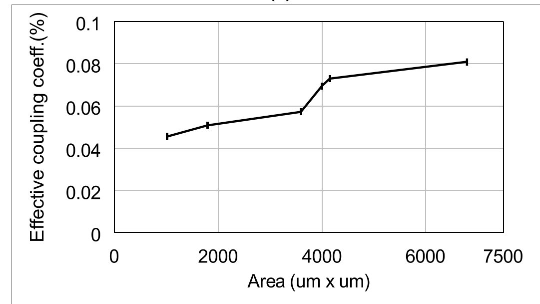

(b)

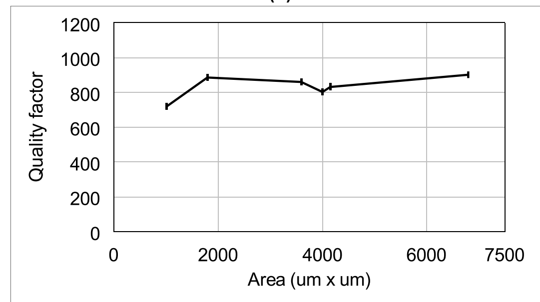

(c)

FIGURE 11. The SAW resonator parameters as a function of the IDT area extracted from experimental results: (a) static capacitance C_o; (b) effective coupling factor k^2_{eff}; (c) mechanical quality factor Q_m.

and the final value of the extracted model parameter is the mean value of all measurements (extreme values due to local defects in the nanometric IDTs were excluded).

As expected, the static capacitance is directly proportional to the area, varying from 0.2 pF for an area of 1000 μm^2 to 1 pF for an area of 6800 μm^2 (Fig.11 (a)). The quality factor is practically independent of the area with a mean value of 830 (Fig.11 (b)). The effective coupling coefficient (Fig.11 (c)) shows an unexpected dependency on the resonator area. This can be due to the edge effects on the static capacitance due to the fact that different areas were obtained for different lengths of the digits. The extracted values for the loss resistances R_s and R_o are between 2…6 Ω. It was not possible to find a correlation between these values and the SAW resonator area.

IV. DESIGN OF LUMPED-ELEMENT SAW RESONATOR BAND PASS FILTER

The schematic of the new PI-type lumped-element SAW resonator band pass filter is shown in Fig.12. The horizontal (series) branch consists of a SAW resonator in parallel with the inductor L_{par} that controls the parallel resonance frequency. The vertical (parallel) branch has a SAW resonator in series with inductor L_{ser} that control the series resonance frequency.

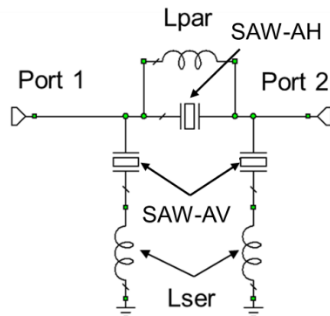

FIGURE 12. PI-type band pass filter with lumped-element SAW resonators.

The design guidelines in the new approach are:

- SAW resonators have the same digit width (w) and digit separation (s), therefore they have the same series resonance frequency f_s. The lumped-elements SAW resonance frequencies will be controlled by L_{ser} and L_{par} (these are the first two independent design variables).

- The design independent variable for the SAW resonators is the IDT area: AH for the horizontally placed resonator and AV for the vertically placed resonator. This variable controls the C_o parameter of each resonator (namely C_{oH} and C_{oV}, respectively). The other two parameters (Q_m and k_{eff}^2) will be considered constant in the design, with values close to those extracted from experimental results.

- Because it is not possible to obtain a direct closed form formula, the design approach is based on "optimization using parametric simulations". In this approach, different values for the design variables are used in repeated simulations and the user selects the optimum frequency response as a tradeoff between insertion/return losses and the out-of-band rejection. Therefore there will not be a unique optimum design solution.

- The dielectric and conductive losses will be included later in the design to evaluate their effect on the filter frequency response.

In the present work, the digit width and separation are $w = s = 200$ μm and a mean value of 5.493 GHz was extracted for the series resonance frequency from the measurements of the test structures.

After a first estimation of L_{ser} and L_{par} using (12)-(15) and the results from Fig.5 (b) and Fig.7 (b), the circuit from Fig.12 was optimized using AWR MWO and parametric simulations. The S parameter results for the designed circuit are shown in Fig.13. The final values for the four independent variables are: $C_{oH} = 0.938$ pF, $C_{oV} = 0.615$ pF, $L_{ser} = 1.37$ nH, $L_{par} = 0.92$ nH. The other model parameters are: $f_{ser} = 5.493$ GHz, $Q_m = 830$, $k_{eff}^2 = 0.1\%$, $R_s = 4$ Ω, $R_o = 4$ Ω (see section III.B).

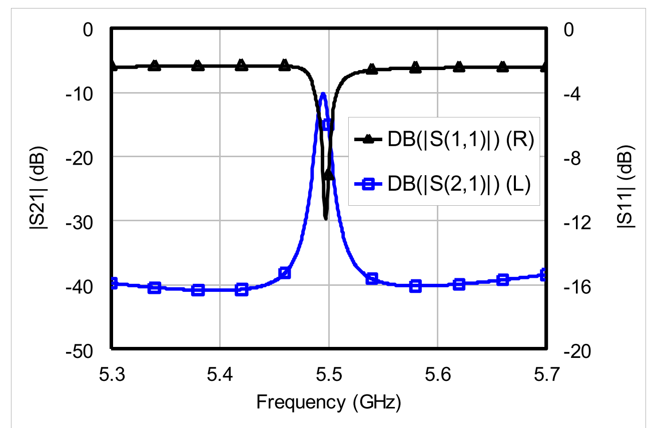

FIGURE 13. Simulated S parameters for the optimized filter ($C_{oH} = 0.938$ pF, $C_{oV} = 0.615$ pF, $L_{ser} = 1.37$ nH, $L_{par} = 0.92$ nH).

The next step consists of the planar inductors design and filter layout optimization. Since the operating frequency range is above 5 GHz, full wave electromagnetic modeling and simulations are mandatory. The inductors and filter electromagnetic models were developed using the commercial software package Mentor Graphics HyperLynx full-wave solver (https://www.mentor.com/pcb/hyperlynx/full-wave-solver/).

The dielectric layer configuration from Fig.2 was modeled as follows: high-resistivity silicon layer $\varepsilon_r = 11.9$, buffer layer and GaN layer $\varepsilon_r = 9.0$. Dielectric losses were neglected. In the case of the inductors, for a metallic strip with a width of 40 μm and a thickness of 0.3 μm gold metallization, a value of about 0.6 nH/mm was extracted from electromagnetic simulations.

The gold conductivity was set to $4 \cdot 10^7$ S/m. Then the length of the inductors was estimated to 2.3 mm for L_{ser} and 1.5 mm for L_{par} and they will be adjusted during the design process. These planar inductors were folded and the layout of the lumped-elements SAW resonator band pass filter is presented in Fig. 14.

Because of the U shape of the inductors, the presence of the ground planes of the CPW lines for the input and the output

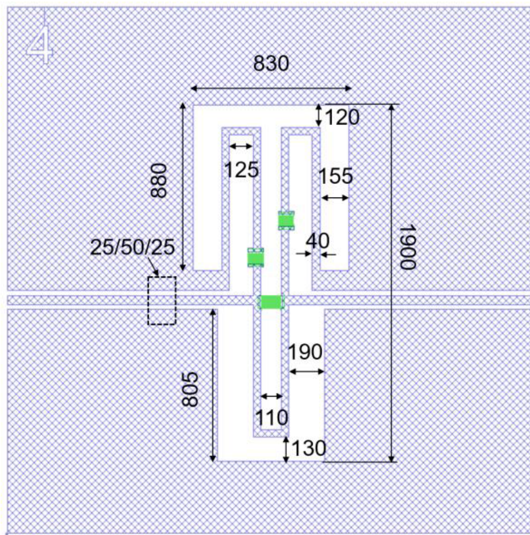

FIGURE 14. Optimized layout of the proposed lumped-elements SAW resonator band pass filter (dimensions given in micrometers; SAW resonators in green).

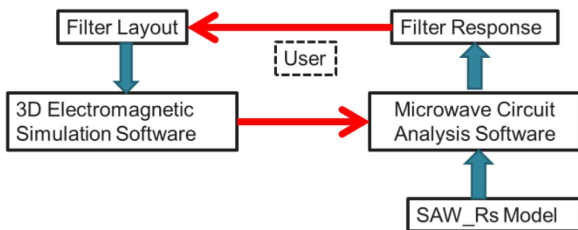

FIGURE 15. The electromagnetic co-simulation based optimization flow chart.

of the filter and due to the high operating frequency, an electromagnetic co-simulation based optimization technique was implemented. This approach requires the co-simulation of the filter layout and the SAW resonator model in the frame of a microwave circuit analysis software (AWR MWO).

The optimization flow chart is illustrated in Fig.15. The filter layout is simulated using Mentor Graphics HyperLynx full-wave solver. In the layout the SAW resonators are replaced by the internal ports feature. The S-parameters are then exported in the Touchstone format considering the two ports used at the input and output of the filter and the internal ports corresponding to the SAW resonators (a total number of 5 ports corresponding to a ∗.s5p file).

The AWR MWO will link the electromagnetic simulated results to the equivalent circuit model for the SAW resonator. The schematic used for the filter design is shown in Fig. 16. The circuit block with 5 ports represents the filter layout simulation results. The circuit blocks "RezV" and "RezH" model the SAW resonator with the mBVD equivalent circuit model from Fig.3 with the current values for C_o and other model parameters introduced in Section II.A.

The AWR MWO provides the filter frequency response as return losses at the input/output external ports and the

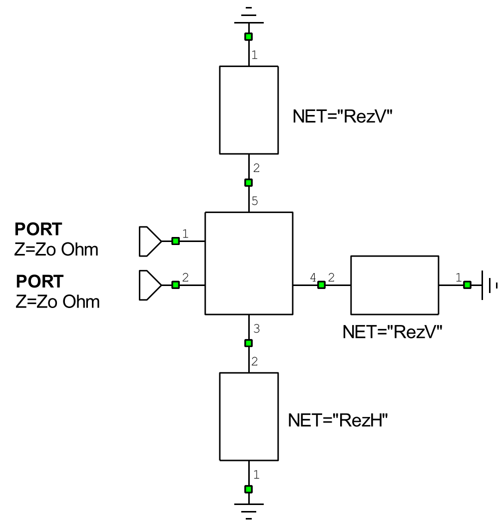

FIGURE 16. AWR MWO schematic used for filter design (see text).

transmission between the two external ports. The user evaluates the filter response and decides what layout parameter should be changed to improve it.

The main decisions of the user are related with: minimum insertion losses; out-of-band rejection; filter matching. These requirements are difficult to be integrated into a multi-objective error function and an automatic optimization because it is difficult to define realistic desired responses that fit with the lumped-element SAW resonator properties as well as realistic weight coefficients.

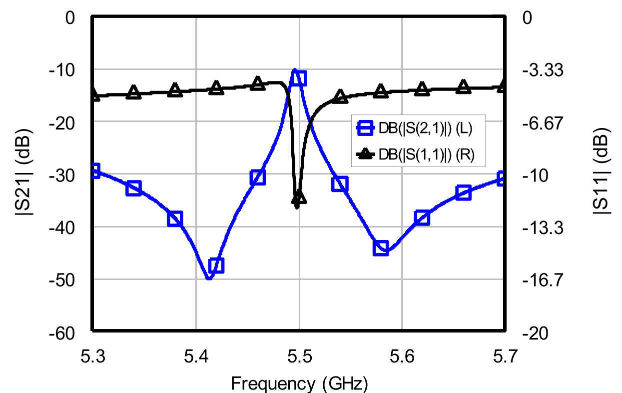

FIGURE 17. Simulated S parameters for the optimized filter, for C_{oH} = 0.95 pF, C_{oV} = 0.59 pF and the layout dimensions from Fig.14.

The optimized layout dimensions are presented in Fig.14. The input and output CPW lines have gap-width-gap of 25-50-25 μm (approximately 50 Ω characteristic impedance). The overall filter dimensions are 0.83 mm × 1.9 mm. For future packaging purposes two CPW lines were added to the filter, leading to a final chip size of 2.8 mm × 2.8 mm. The simulated results for the final version of the design are shown in Fig.17. The optimized values for the independent variables are: C_{oH} = 0.95 pF, C_{oV} = 0.59 pF. The other model parameters have the same values as

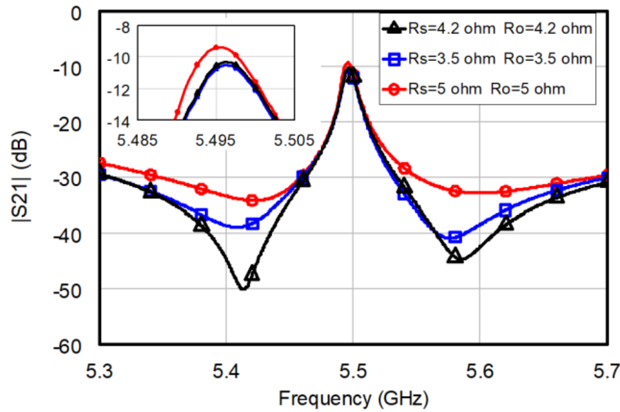

FIGURE 18. The effect of the variation of R_S and R_O on the filter transmission parameter |S21|.

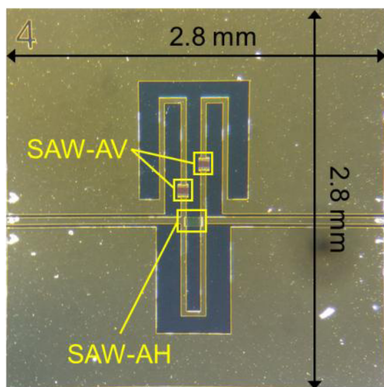

FIGURE 19. Optical photo of the fabricated lumped-element SAW band pass filter.

those used for the circuit optimization (ie. $f_s = 5.493$ GHz, $Q_m = 830$, $k^2_{eff} = 0.1\%$, $R_s = 4.2\ \Omega$, $R_o = 4.2\ \Omega$). The simulated insertion losses are 10.32 dB at central operating frequency of 5.4965 GHz, the 3 dB bandwidth is 10.2 MHz (0.18%), the out-of-band rejection is 34.1 dB @ 5.589 GHz. The effect of the change in the R_s and R_o is presented in Fig.18. The insertion losses and the bandwidth are not affected, but the out-of-band rejection is significantly reduced.

V. EXPERIMENTAL VALIDATION

The lumped-element SAW resonator band pass filters were fabricated with the technological flow presented in section III.A. The photo of the fabricated filter structure is shown in Fig.19. According to the values of C_{oH} and C_{oV} resulted from the design, the horizontal SAW resonator (SAW-AH) has 170 digits with a length of 100 micrometers and the vertical SAW resonator has 200 digits with a length of 50 micrometers. A SEM image of one the vertical SAW resonator is shown in Fig. 20 (a) and a detail of the 200 nm wide digits in Fig. 20(b). Using the described technological approach, uniform high quality 200 nm digits were obtained.

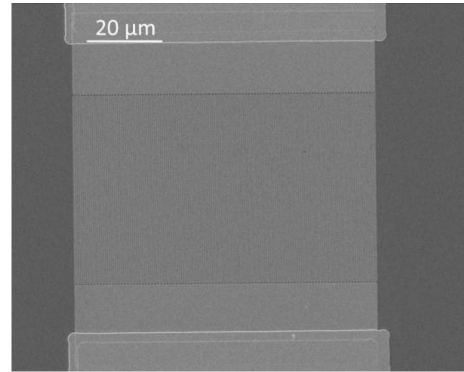

(a)

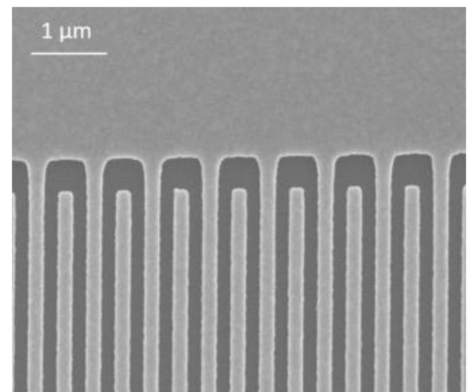

(b)

FIGURE 20. Fabricated SAW-BPF: (a) SEM image of one of the vertically connected SAW resonators; (b) SEM detail of the 200 nm wide digits.

TABLE 1. SAW resonator model parameters.

Parameter	Design	Measurement
f_{ser} [GHz]	5.493	5.493
C_{oH} [pF]	0.95	0.88
C_{oV} [pF]	0.590	0.596
k_{eff}^2 [%]	0.1	0.07
Q_m	830	830
R_s [Ω]	4.2	4.4
R_o [Ω]	4.2	5.4

TABLE 2. SAW Band-pass filter performance.

BPF Parameter	Design	Measurement
Insertion losses [dB]	10.32	12.87
Out-of-band rejection [dB]	34.1	24.1
Return loss [dB]	12.2	16.35
3dB bandwidth [MHz]	10.2	8.3
Central frequency [GHz]	5.4965	5.4938

The S parameters for the fabricated filter structures were measured on-wafer using a Vector Network Analyzer from Anritsu. The experimental results are compared with the simulated ones in Fig.21 (a) (|S21| parameter) and Fig.21(b) (|S11| parameter). The SAW resonator model parameters

TABLE 3. Comparison of SAW band-pass filter processed on GaN on substrate performance with the state of the art.

BPF Parameter	[8]	[9]	[10]	[2]	This work
Insertion losses	25.5 dB/24.4 dB	14 dB	27 dB/35 dB	33 dB	12.87 dB
Return loss	8.5/10 dB.	N.A.	N.A.	0.4 dB	16.3 dB
Out of band rejection	~35 dB	15 dB	23 dB/15 dB	10 dB	24.17 dB
-3dB bandwidth	N.A.	20.2 MHz	N.A.	N.A.	8.3 MHz
Central frequency	237.8 MHz/349.7 MHz	2.1 GHz	1.625 GHz/ 2.25 GHz	5.64 GHz	5.49 GHz
Observation	Delay lines /Fe-doped GaN on sapphire	Resonator on membrane	GaN/ sapphire	Delay line GaN/Si	Lumped-element SAW resonator on GaN/Si

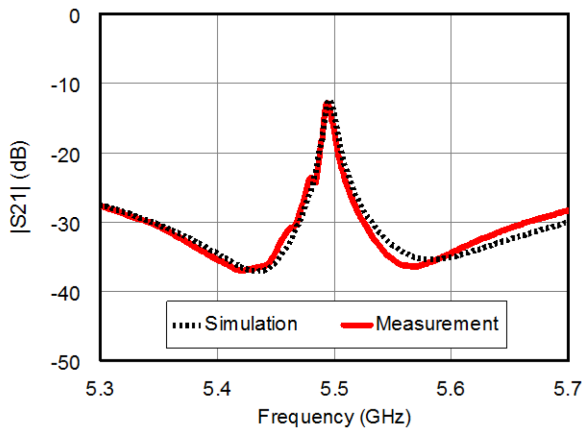

(a)

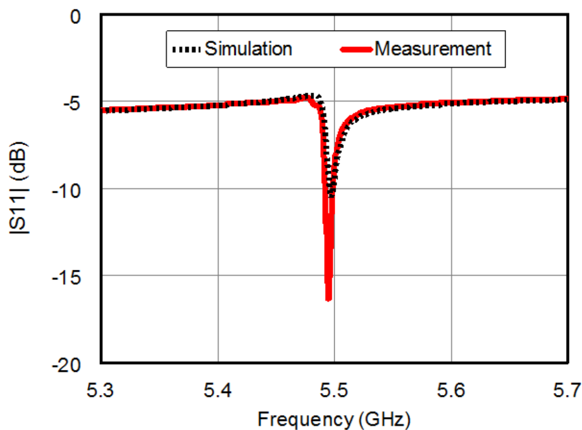

(b)

FIGURE 21. Simulated vs. Measured SAW-BPF S-Parameters: (a) transmission parameter (|S21|); (b) reflection parameter (|S11|).

values were slightly adjusted for the best curve fitting. These values are presented in Table 1 and they are compared with the final values from the design (section IV). A decrease of the effective coupling coefficient (k_{eff}^2) from 0.1 % to 0.07 %, a decrease of the static capacitance of the horizontal SAW resonator (C_{oH}) and a slight increase of losses were observed.

The designed (section IV) and measured band pass filter characteristic performances are compared in Table 2. Because of the decrease of the effective coupling coefficient (k_{eff}^2), the insertion losses increased with 2.55 dB and the 3 dB bandwidth decreased from 10.2 MHz (simulated in the design) to 8.3 MHz (measured). The out-of-band rejection decreased due to the increase of losses.

A comparison of the filter performances reported in this work and the current state of the art for SAWs processed on GaN is presented in Table 3. Since there are relatively few publications reporting microwave SAW filters processed on GaN, related work was also considered. The insertion losses are higher than reported in the current work, even in the case of [9], where the operating frequency is much lower (2.1 GHz) and the resonator is processed on a 10 μm thick silicon membrane. The rejection is also poorer or comparable to the one reported in the present work, except for [8], where the GaN layer was doped with iron and the configuration is of delay line type, with very high insertion losses (around 25 dB).

VI. CONCLUSIONS

A new approach in the development of band pass GaN/Si SAW impedance element filters operating in the few GHz region was presented. The basic building blocks are lumped-element SAW resonators tuned with series/parallel connected planar inductors processed on the same GaN/Si substrate. The SAW resonator is modeled using a new approach based on 4 model parameters (series resonance frequency, static capacitance, quality factor, effective coupling coefficient) originating from its physical behavior.

The SAW resonators were fabricated using electron beam lithography on a GaN on Si substrate with a GaN layer thickness of 1 μm and 200 nm wide digits, corresponding to a series resonance frequency (f_s) of 5.493 GHz. A quality factor (Q_m) of 830 and an effective coupling coefficient (k_{eff}^2) of 0.07% were extracted from measured data.

As a proof of concept, a PI-type filter with coplanar waveguide transmission line input and output was designed using full-wave electromagnetic and circuital co-simulations and parametric optimizations.

For the fabricated band pass filter the measured characteristics are: insertion losses of 12.9 dB at 5.49 GHz, return losses of 16 dB, 3 dB bandwidth of 8.3 MHz, out-of-band rejection of 24 dB. These parameters represent the best performances reported to date for SAW band pass filters on GaN/Si operating above 5 GHz.

The filter is very compact with an effective area of only 0.83 mm x 1.9 mm and is compatible to be monolithic integrated with GaN active electronics. The fabricated filter can be diced and used as a standalone component.

REFERENCES

[1] M. Rais-Zadeh *et al.*, "Gallium nitride as an electromechanical material," *J. Microelectromech. Syst.*, vol. 23, no. 6, pp. 1252–1271, Dec. 2014, doi: 10.1109/JMEMS.2014.2352617.

[2] A. Müller *et al.*, "SAW devices manufactured on GaN/Si for frequencies beyond 5 GHz," *IEEE Electron Device Lett.*, vol. 31, no. 12, pp. 1398–1400, Aug. 2010, doi: 10.1109/LED.2010.2078484.

[3] A. Müller *et al.*, "Sezawa propagation mode in GaN on Si surface acoustic wave type temperature sensor structures operating at GHz frequencies," *IEEE Electron Device Lett.*, vol. 36, no. 12, pp. 1299–1302, doi: 10.1109/LED.2015.2494363.

[4] A. Müller *et al.*, "GaN membrane supported SAW pressure sensors with embedded temperature sensing capability," *IEEE Sensors J.*, vol. 17, no. 22, pp. 7383–7393, Nov. 2017, doi: 10.1109/JSEN.2017.2757770.

[5] U. C. Kaletta *et al.*, "$AlN/SiO_2/Si_3N_4/Si(100)$-Based CMOS compatible surface acoustic wave filter with −12.8-dB minimum insertion loss," *IEEE Trans. Electron Devices*, vol. 62, no. 3, pp. 764–768, Mar. 2015, doi: 10.1109/TED.2015.2395443.

[6] D. Morgan, *Surface Acoustic Wave Filters*. Amsterdam, The Netherlands: Elsevier, 2007.

[7] K.-Y. Hashimoto, *Surface Acoustic Wave Devices in Telecommunications: Modelling and Simulation*. New York, NY, USA: Springer-Verlag, 2000.

[8] Y. Fan *et al.*, "Surface acoustic waves in semi-insulating Fe-doped GaN films grown by hydride vapor phase epitaxy," *Appl. Phys. Lett.*, vol. 105, no. 6, p. 062108, 2014, doi: 10.1063/1.4893156.

[9] A. Ansari, V. J. Gokhale, V. A. Thakar, J. Roberts, and M. Rais-Zadeh, "Gallium nitride-on-silicon micromechanical overtone resonators and filters," in *IEDM Tech. Dig.*, Washington, DC, USA, Dec. 2011, pp. 20.3.1–20.3.4, doi: 10.1109/IEDM.2011.6131590.

[10] T. Palacios *et al.*, "High frequency SAW devices on AlGaN: Fabrication, Characterization and integration with optoelectronics," in *Proc. IEEE Ultrason. Symp.*, Munich, Germany, Oct. 2002, pp. 57–60, doi: 10.1109/ULTSYM.2002.1193352.

[11] A. C. Bunea, A. M. Dinescu, L. A. Farhat, C. Pârvulescu, and D. Neculoiu, "Effect of key technological parameters on GaN/Si SAW resonators operating above 5 GHz," *Romanian J. Inf. Sci. Technol.*, vol. 20, no. 4, pp. 354–368, 2017.

[12] D. Psychogiou, R. Gómez-García, R. Loeches-Sánchez, and D. Peroulis, "Hybrid acoustic-wave-lumped-element resonators (AWLRs) for high-Q bandpass filters with quasi-elliptic frequency response," *IEEE Trans. Microw. Theory Techn.*, vol. 63, no. 7, pp. 2233–2244, Jul. 2015, doi: 10.1109/TMTT.2015.2438894.

[13] D. Psychogiou, R. Gómez-García, and D. Peroulis, "Coupling-matrix-based design of high-Q bandpass filters using acoustic-wave lumped-element resonator (AWLR) modules," *IEEE Trans. Microw. Theory Techn.*, vol. 63, no. 12, pp. 4319–4328, Dec. 2015, doi: 10.1109/TMTT.2015.2494597.

[14] D. Psychogiou, R. Gómez-García, and D. Peroulis, "Constant in-band group-delay acoustic-wave-lumped-element-resonator-based bandpass filters and diplexers," *IEEE Trans. Microw. Theory Techn.*, vol. 66, no. 5, pp. 2199–2209, May 2018, doi: 10.1109/TMTT.2018.2801824.

[15] A. C. Bunea, D. Neculoiu, and A. Dinescu, "GaN/Si monolithic SAW lumped element resonator for C- and X- band applications," in *Proc. IEEE Asia–Pacific Microw. Conf.*, Kuala Lumpur, Malaysia, Nov. 2017, pp. 1010–1013.

[16] A. A. Oliner, *Acoustic Surface Waves*. New York, NY, USA: Springer-Verlag, 1978;.

[17] S. V. Biryukov, Y. V. Gulyaev, V. V. Krylov, and V. P. Plessky, *Surface Acoustic Waves in Inhomogeneous Media*. New York, NY, USA: Springer-Verlag, 1995.

[18] C. Campbell, *Surface Acoustic Wave Devices and Their Signal Processing Applications*. New York, NY, USA: Academic, 1989.

[19] J. D. Larson, III, P. D. Bradley, S. Wartenberg, and R. C. Ruby, "Modified Butterworth-van Dyke circuit for FBAR resonators and automated measurement system," in *Proc. IEEE Ultrason. Symp.*, vol. 1, Oct. 2000, pp. 863–868.

[20] *IEEE Standard on Piezoelectricity*, ANSI/IEEE Standard 176-1987, 1988, p. 51.

[21] B. Aronov, "On the optimization of the effective electromechanical coupling coefficients of a piezoelectric body," *J. Acoust. Soc. America*, vol. 114, no. 2, pp. 792–800, 2003, doi: 10.1121/1.1592163.

DAN NECULOIU (M'06) graduated the Faculty of Electronics, Politehnica University of Bucharest, in 1985. He received the Ph.D. degree in nonlinear microwave circuits modeling in 1997. Since 2004, he has been a Full Professor with the Faculty of Electronics, Telecommunications and Information Technology, Politehnica University of Bucharest, where he teaches the undergraduate courses, electron devices and electronic circuits, and the master courses, RF MEMS and microwave devices and circuits. He is currently also a Principal Researcher with the National Institute for Research and Development in Microtechnologies. He was the Head of the Romanian Team in the FP7 STREP project, MEMS-4-MMIC, and ERA-NET project, MEMIS. He has authored over 150 research papers published in journals and conference proceedings. His main research areas are the modeling, simulation, design, measurement, and characterization of a wide range of microwave- and millimeter-wave devices, components, circuits, and subsystems, including membrane supported filters, antennas and receiver modules, AlN and GaN piezoelectric devices and circuits based on FBARs and surface acoustic waves in the microwave frequency range, CNT and graphene devices and circuits, RF MEMS switches, and AIIIBV devices.

ALINA-CRISTINA BUNEA (S'10–M'16) was born in Bucharest, Romania, in 1986. She received the B.Sc., M.Sc., and Ph.D. *(magna cum laude)* degrees in electronics from the Politehnica University of Bucharest, Romania, in 2009, 2011, and 2016, respectively. She is currently a Senior Research Scientist with the National Institute for Research and Development in Microtechnologies, where she is involved in the design, 3-D electromagnetic modeling, and characterization of passive and active microwave circuits. Her interests include microwave- and millimeter-wave circuits, LTCC circuits, microwave circuits based on surface acoustic wave components, and the design and characterization of graphene-based microwave devices.

ADRIAN M. DINESCU received the M.Sc. and Ph.D. degrees in solid state physics from the Faculty of Physics, University of Bucharest, in 1993 and 2010, respectively.

From 1993 to 1997, he was with the National Institute for Electronic Components Research, where he was involved in the field of optoelectronics components. Since 1997, he has been with the National Institute for Research and Development in Microtechnologies, where he is currently the Head of the Nanoscale Structuring and Characterization Laboratory. He was a project coordinator in eight national projects, and the coordinator of Romanian partner (National Institute for Research and Development in Microtechnologies) of the CATHERINE FP7 project, JRP Romania–Bulgaria (Nanostructured and amorphous semiconductor films for sensors application, running), and M-ERA.NET PhotoNanoP. He is involved in the microscale and nanoscale characterization using FE-SEM and in structuring at the nanoscale using electron beam lithography. He has co-authored over 75 papers in ISI journals. His expertise also includes micro- and nano-fabrication and optoelectronic measurements.

Dr. Dinescu received the Gheorghe Cartianu Prize from the Romanian Academy in 2016.

LEO A. FARHAT received the Ph.D. degree in microwave engineering from Telecom Bretagne, Brest, France, in 2011. He was with the Laboratory of Sciences and Techniques of Information, Communication and Knowledge, Telecom Bretagne, where his research activities concerned the numerical modeling of electromagnetic wave propagation in anisotropic media. From 2011 to 2015, he was a Research and Development Engineer with Cobham Microwave, Villebon-sur-Yvette, France, where his development activities concerned ferrite devices as circulators, isolators, and phase shifters mainly for space applications. Since 2015, he has been with the Data System & Microelectronics Division, European Space Agency (ESA), as a Component Engineer. He currently provides technical expertise to ESA missions in the selection, procurement, design, characterization, evaluation, and qualification of passive components. In parallel, he prepares, implements, and manages R&D and ESCC qualification activities funded by ESA programs.